

Simulation of frictional effects in models for calculation of the equilibrium state of flexible pipe armouring wires in compression and bending

Niels Højen Østergaard, Anders Lyckegaard and Jens H. Andreasen

Summary. The motivation for the work presented in this paper is a specific failure mode known as lateral wire buckling occurring in the tensile armour layers of unbounded flexible pipes. Such structures are steel-polymer composites with a wide range of applications in the offshore industry. The tensile armour layers are usually constituted by two layers of oppositely wound steel wires. These may become laterally unstable when a flexible pipe is exposed to repeated bending cycles and longitudinal compression.

In order to model the mechanical behavior of the armouring wires within the pipe wall, a formulation based on the equilibrium of a curved beam embedded in an initially cylindrical surface bent into a toriod is applied. In the present work, the response of a single armouring wire subjected to compression and cyclic bending will be studied, in order to detect lateral buckling of the wire. Frictional effects are included as distributed tangential and transverse loads based on a simple regularized Coulomb model.

Key words: curved beam equilibrium, wire mechanics, friction, flexible pipes, lateral buckling of armour wires

Introduction

Unbounded flexible pipes are steel-polymer composite structures with a wide range of applications in the offshore industry. A flexible pipe structure is usually constituted by numerous layers with different properties, see Figure 1. The pipe bore, denoted the carcass, is constituted by helically wound profiles surrounded by a pressure armour. These layers ensure the structural integrity against external and internal pressure. The pressure armour is surrounded by a polymeric liner, which like the external pipe sheath, is a fluid barrier layer. The space between liner and outer sheath is usually denoted the 'pipe annulus'. In the pipe annulus, the tensile armour layers are located, usually constituted by two layers of oppositely wound steel wires. Usually, the total number of wires is 80 – 150. These layers ensure the structural integrity against longitudinal and torsional loads. The tensile armour layers are in flexible pipes for deep-water applications usually surrounded by a high strength tape in order to prevent radial deflections. Flexible pipes are usually designed in accordance with the specifications given in the API17J-standard, [1].

In the present paper, only the mechanics of the tensile armour wires are addressed. During pipe laying, the flexible pipe is in a free-hanging configuration from an installation vessel to the seabed, see Figure 3. Furthermore, the pipe is empty, in order to ease the installation process, and hydrostatic pressure on the end cap causes longitudinal

compression. Due to vessel movements, wave loads and current the flexible pipe is also exposed to repeated bending cycles. This is known possibly to lead to lateral wire buckling failure, especially, if the outer sheath of the pipe is breached such that the pipe annulus is flooded. This leads to, that external pressure no longer induce sufficient frictional resistance to prohibit wire slippage. The failure mode was first described by Braga and Kaleff, [2], who reproduced it experimentally in the laboratory. Further experimental investigations were conducted in [3]-[6].

In repeated bending the wires within the pipe wall may slip towards a configuration in which the wire lay angle is not constant, like in the initial helical configuration. For a pipe subjected to longitudinal compression, the geometrical configurations of the wires obtained after a significant number of bending cycles, may be associated with wire buckling within the pipe wall leading to a reduced load carrying ability of the pipe structure.

The mechanics of armouring wires in flexible pipes have been subject of both academic and industrial research in the past few decades. Féret and Bournazel, [7], derived expressions for prediction of the global response of straight flexible pipes on basis of analysis of internal components. The methods were implemented in a computerprogram, see [8], in which the armouring tendons were described as perfect helices. The global behavior of flexible pipes has been investigated further in numerous publications, see [9]-[12].

Witz and Tan, [13], and Kraincanic and Kabadze, [14], considered progression of wire slippage along curves with constant lay angles for flexible pipes in bending. Sævik, [16], addressed the same problem, but based his analysis on a finite element formulation based on finite-strain continuum mechanics. Out and von Morgen, [15], considered wire slip towards the geodesic of a toriod in bending. Leroy and Estrier, [17], simulated wire slippage due to cyclic bending based on curved beam equilibrium with frictional effects taken into calculation. However, a prescribed experience-based solution form was applied.

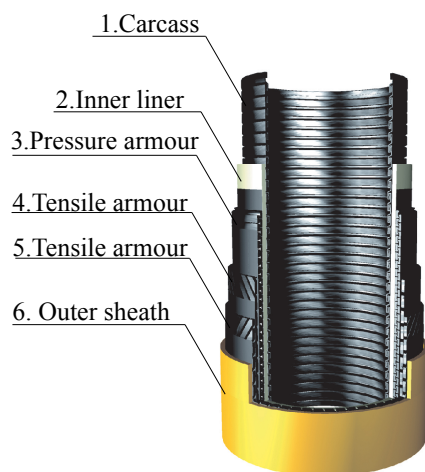


Figure 1. Flexible pipe design.

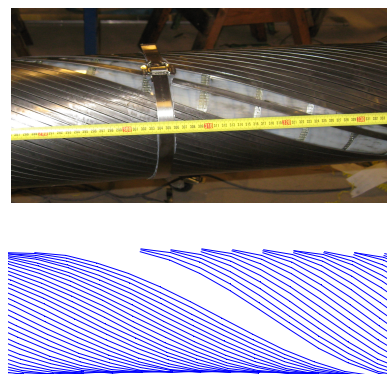


Figure 2. Buckling mode, triggered experimentally and simulated.

The approaches to wire mechanics are obviously all incapable of predicting transverse wire slippage for a flexible subjected to bending and compression. A method for calculation of the equilibrium state of a wire which was free of geometrical constraints was proposed in [6] and elaborated further in [18]. The problem of a curved beam embedded in a frictionless toroid was addressed, assuming that the wire equilibrium state reached after

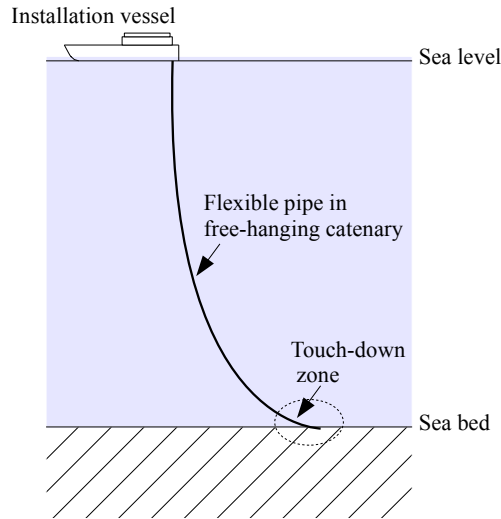


Figure 3. Principle drawing, flexible pipe during installation.

a significant number of bending cycles when friction is present, is reached instantaneously when the wire is loaded, if friction is neglected. The proposed method was applied to the lateral buckling problem, see [6], in which it was shown that the method was capable of representing the buckling modes of deformation. An example of simulated and experimentally triggered buckling modes is presented in Figure 2. The governing equations were formulated analytically, but solved by numerical means. However, frictional effects were not investigated. Since transverse wire stabilization due to friction may possibly increase the buckling load and shorten the modes of deformation, frictional effects are included in the present approach. For the sake of simplicity, only a single wire within the wall of a flexible pipe subjected to compression and repeated bending cycles will be analyzed, since frictional effects on all wires and arising couplings to the global constitutive behavior of flexible pipes demands severe computational power.

In the present approach, the focus has mainly been on adding some frictional stabilization in order to study, how this influences the wire responses, rather than to model an exact physical behavior with a frictional law based on experimentally obtained parameters. Despite results may not correlate well with experimental measurements, the chosen theoretical approach and the obtained results is of a very interesting nature due to, that very little research in the mechanics of wire slippage is available.

Single wire mechanics

System of field equations

In this section, the system of field equations governing the wire equilibrium state is presented. The system of equations was derived in [6] and [18], but for the sake of completeness the derivation is summarized in the Appendix. The wire geometry is shown in Figure 4 with a curvilinear (tnb) coordinate frame. Before proceeding, the assumptions on which the present formulation is based are summarized

- The wire will in the initial configuration be assumed to constitute a geodesic on a cylinder, hence, a helix.

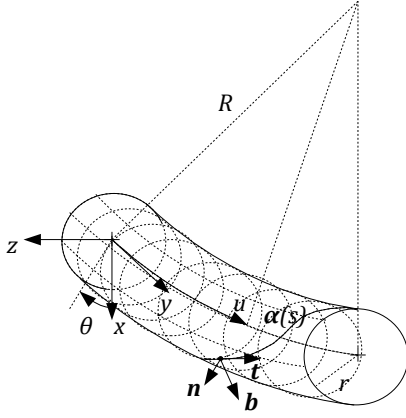


Figure 4. Wire geometry.

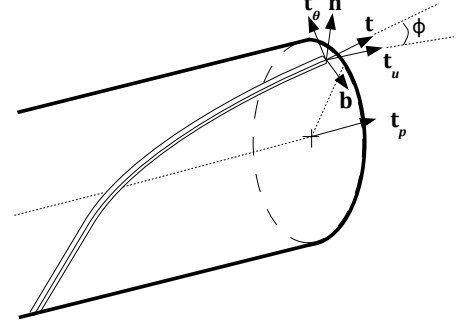


Figure 5. Wire coordinate triads.

- The pipe will be assumed bent to a constant radius of curvature. Hence, a wire constitutes a curve on a cylindrical surface, which is bent into a toroid with major radius $R = 1/\kappa$.
- A wire will be modeled as a long and slender curved beam of rectangular cross section. The dimensions of the cross sections are assumed small compared to both minor and major torus radii.
- Wire friction will be modeled using Coulombs law. Hence, the frictional load is assumed speed independent.
- Wire inertia terms are neglected, since these are estimated small compared to stiffness related terms. A similar approach was followed in [17].
- The wires in the inner layer of tensile armour have responses which in terms of stable/unstable behavior are sufficiently equivalent to only consider a single armouring wire.

Frictional effects will be accounted for by applying transverse loads. However, since inertia terms are small, second order terms related to the wire slip acceleration in the equilibrium equations will be neglected. Furthermore, applying Coulomb friction, the transverse wire loads constituting frictional effects are governed only by the normal wire load and the frictional coefficient. The direction of the frictional loads will be determined on basis of the previous load step.

Six differential equations in torus coordinates u and θ , wire lay angle ϕ , tangential wire force P_t , Shear force in the binormal wire direction P_b and normal moment M_n as functions of wire arclength s is derived.

$$\frac{du}{ds} = \frac{\cos \phi}{1 + r\kappa \cos \theta} \quad (1)$$

$$\frac{d\theta}{ds} = \frac{\sin \phi}{r} \quad (2)$$

$$\frac{d\phi}{ds} = -\frac{\kappa \sin \theta}{1 + r\kappa \cos \theta} \cos \phi + \kappa_g \quad (3)$$

$$\frac{dP_t}{ds} = \kappa_n P_n - \kappa_g P_b - p_t \quad (4)$$

$$\frac{dP_b}{ds} = \kappa_g P_t - \tau P_n - p_b \quad (5)$$

$$\frac{dM_n}{ds} = -\kappa_n M_t + \tau M_b + P_b \quad (6)$$

The system is derived on basis of Kirchoff's equations for curved beam equilibrium given on vectorial form by Reissner, [19], and concepts from differential geometry for mathematical description of curves on surfaces.

In order to discretize the system on a known regular mesh, the unknown arclength s in the deformed state is converted to initial helical arclength s_0 . Assuming strains small, this can be done by applying Cauchy's definition of strain, ϵ , which is given by

$$\frac{ds}{ds_0} = (1 + \epsilon) \quad (7)$$

The initial arclength is given by the well-known relation valid for a helix

$$s_0 = \frac{r\theta}{\sin(\phi_{\text{hel}})} \quad (8)$$

in which ϕ_{hel} is the initial wire lay angle.

The system will be solved with respect to boundary conditions corresponding to the physics of a wire within the wall of a flexible pipe

$$u(0) = 0 \quad \theta(0) = \theta_{\text{ini}}^A \quad \phi(0) = \phi_{\text{hel}} \quad (9)$$

$$P_{\text{app}} = P_t \cos \phi + P_b \sin \phi \quad \theta(S_L) = \theta_{\text{ini}}^B \quad \phi(S_L) = \phi_{\text{hel}} \quad (10)$$

in which P_{app} is the external load on the wire in the longitudinal pipe direction and S_L is the total arclength of the wire. θ_{ini}^A and θ_{ini}^B denotes the circumferential wire angles in both end of the pipe.

Wire stability in dynamic bending

Stability problems have to a wide extend been investigated and are well-described in the literature. In general, compressive loads are known possibly to cause the equilibrium equations of a given structure to be fulfilled in buckled geometrical configurations associated with large deflections and rotations. The corresponding equilibrium paths in force-displacement diagrams may exhibit softening, bifurcation or limit point behavior. Neglecting friction on the wires, a classical stability approach to the lateral wire buckling problem was followed in [6]. In the present approach, simulation of frictional loads encaptures an additional physical effect, namely, that cyclic loads must be applied in order for the wire to slip. A different definition of stability must therefore be considered. Considering the equilibrium paths of a point on the modeled wire, these will, except for the points $s = 0$ and $s = S_L$, exhibit a 'loop-like' behavior (examples of such loops are given

in Figure 11 and 12). If the wire when subjected to cyclic loads converges towards an equilibrium state in which this loop is closed, the wire will in the following be considered stable. If this is the case, the pipe strain obtained by the analysis after each bending cycle has been completed, will be constant after a number of bending cycles have been applied. On the other hand, if the (load-strain) loops are not closed, the slip with respect to the initial configuration will increase for each bending cycle. This may lead to, that the yield strength of the wire steel is exceeded and failure occurs due to formation of plastic hinges.

In [6] it was demonstrated that buckling could be triggered by adding a small harmonic response to the initial helical geodesic curvature, such that κ_g can be determined by

$$\kappa_g = \frac{M_n}{EI_n} + \sum_{i=1}^m \gamma_i \sin\left(\frac{i\pi s}{L}\right) \quad (11)$$

In the following, the imperfection will be calculated by setting $\gamma_{1\dots 20} = -0.001$ in accordance with [6].

Frictional forces

The wire loads in the toroid tangent plane, p_t and p_b , will be defined such that they constitute frictional resistance. In order to do so, the problem will be defined and solved stepwise for a prescribed load history. First, the wire will be loaded longitudinally. Afterwards cyclic bending will be simulated. An example of such a definition of loads is presented in Figure 7 and 8. Since the mass of the wire is small and assuming bending to be applied slowly, inertia terms can be neglected. Coulomb friction is for a given speed v defined as

$$\mathbf{p}_{\text{fric}} \leq -\mu p_n \frac{\mathbf{v}}{\|\mathbf{v}\|} \quad (12)$$

$$(13)$$

The slip speed can be observed only to provide the direction of the frictional force. However, the formulation given in equation (12) is inconvenient for implementation in numerical solvers. A regularization will therefore be applied by assuming a transition, z , between zero frictional force for $v = 0$ to full frictional force at $v = z$

$$v < z : \mathbf{p}_{\text{fric}} = -p(v) \frac{\mathbf{v}}{\|\mathbf{v}\|} \quad (14)$$

$$v \geq z : \mathbf{p}_{\text{fric}} = -\mu p_n \frac{\mathbf{v}}{\|\mathbf{v}\|} \quad (15)$$

in which z is the length of the transition zone and $p(v)$ is a polynomial of second order determined on basis of the conditions

$$p(0) = 0 \quad p(z) = \mu p_n \quad \frac{dp(z)}{dv} = 0 \quad (16)$$

The slip \mathbf{D} is calculated with respect to the previous load step, see Figure 6. For the load step i and the curvature fixed to $\kappa = \kappa_i$ the slip is given by

$$\mathbf{D}(s)_i = \mathbf{x}(s)_i - \mathbf{x}(s)_{i-1} \quad (17)$$

The slip speed can on this basis be calculated as

$$\mathbf{v}(s)_i = \frac{\mathbf{D}_i}{\Delta t} \quad (18)$$

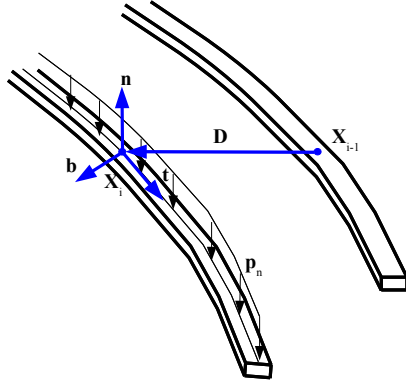


Figure 6. Definition of wire slip, which is calculated with respect to the deformed underlying layer.

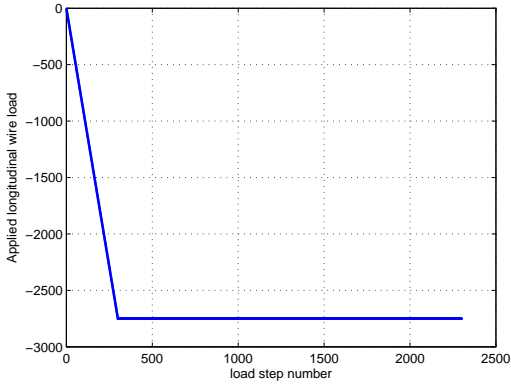


Figure 7. Load history, applied longitudinal wire force.

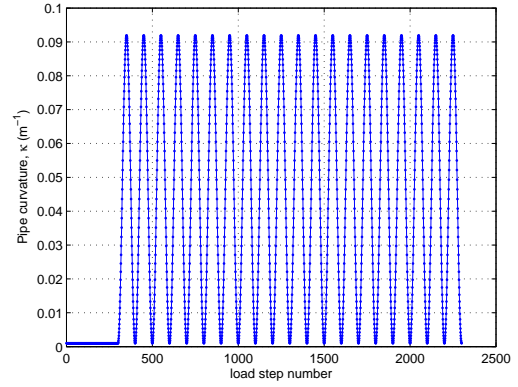


Figure 8. Load history, curvature applied as harmonic response.

With these assumptions, the frictional loads can be calculated as

$$p_{t,i} = \mathbf{p}_{\text{fric},i} \cdot \mathbf{t}_i \quad (19)$$

$$p_{b,i} = \mathbf{p}_{\text{fric},i} \cdot \mathbf{b}_i \quad (20)$$

The normal load is obtained from equation 42 governing the normal force equilibrium

$$p_n = -\frac{dP_n}{ds} - \kappa_n P_t + \tau P_b \quad (21)$$

In the present approach, radial elasticity of the pipe wall being modeled, is not taken into account in an exact manner. Since the effect is crucial to the magnitude of the frictional forces, the minor torus radius will be assumed a function of the applied load. Neglecting ovalization due to bending, the minor torus radius is given by

$$r_d = \left(1 + \frac{\Delta r}{r}\right) r = \left(1 - \frac{k_a \Delta L}{k_r L}\right) r \quad (22)$$

in which k_a and k_r constitute respectively an axial and a radial spring coefficient of the pipe being modeled. This approach is equivalent to the methods described in [7] and are based on the equilibrium of perfect helices. The consequence of calculating the normal

load in this manner is, that p_n is estimated in a fair manner prior to buckling, while the value of p_n may be inaccurate after occurrence of instability, since buckling leads to large changes of wire lay angle.

Since the problem is solved numerically by a commercially available BVP-solver, the length of the slip transition zone, z , must be chosen in such a manner, that convergence can still be obtained. All time steps will be set to $\Delta t = 1$ s. With this assumption, the slip speed is related to the slip by $\mathbf{D}_i = \mathbf{v}_i \cdot [1 \text{ s}]$. By numerical experiments it was determined, that a solution could not be obtained for very short values of z . A transition length of $z = 0.005$ was the smallest value, for which the analysis could be performed with reasonable precision. An obvious consequence of this choice, is that the wires when loaded may not experience full friction, since the slip speed does not cause, that the length of the transition zone is exceeded. In the present analysis, stick effects are therefore simulated in a manner, so the wire has a small speed.

Results

An armoring wire with rectangular cross section within the wall of a flexible pipe will be modeled on basis of the following geometrical input

$$r = 0.2762m \quad L_{\text{pitch}} = 1.474 \text{ m} \quad \phi_{\text{hel}} = 30 \text{ deg} \quad (23)$$

$$\text{width} = 12.5 \text{ mm} \quad \text{height} = 5 \text{ mm} \quad \frac{k_a}{k_r} = 1.9 \quad (24)$$

The wire steel will be considered isotropic with elastic modulus $E = 210$ GPa and Poisson's ratio $\nu = 0.3$. Five analyses will be conducted for compressive wire loads, 2.0 kN, 2.5 kN, 2.75 kN, 3.0 kN and 3.5 kN. 20 bending cycles from $\kappa = 1/1000 \text{ m}^{-1}$ configuration (almost straight) to $\kappa = 1/11 \text{ m}^{-1}$ will be simulated. The frictional coefficient will be set to $\mu = 0.1$, which corresponds well to values chosen in [9] and [17]. The length of the frictional transition zone will be set to $z = 0.005$ m.

Initially, the geometry obtained at the last load step of the simulation will be considered for the compressive load levels 3.0 kN and 3.5 kN, see Figure 9. While the configuration of the wire obtained for the first load level can be observed not to differ significantly from the initial helical shape, the wire configuration obtained for the second load level can be observed to have changed. Obviously, the conclusion can be drawn, that the second load level has caused the wire to exhibit buckling behavior. However, it is not possible solely on this basis to determine, if the first load level considered is stable or not. The wire geometry with maximum curvature for the last simulated bending cycle is shown in Figure 10.

The average pipe strain will now be considered. This is given by

$$\frac{\Delta L}{L} = \frac{u(S_L) - u(0)}{L} \quad (25)$$

In Figure 11 and 12 examples of the loops formed by the equilibrium paths due to cyclic bending are presented. Since it is difficult to draw conclusions regarding stability of these loops, this will be studied on basis of the pipe strain.

In Figure 13 the pipe strain for all analyzed load levels are plotted as functions of the load steps number. Yet, it is still difficult to draw conclusions regarding stability of a specific load level. Furthermore, it is on this basis not possible to draw conclusions regarding if buckling will occur if further bending cycles are applied. Therefore, the

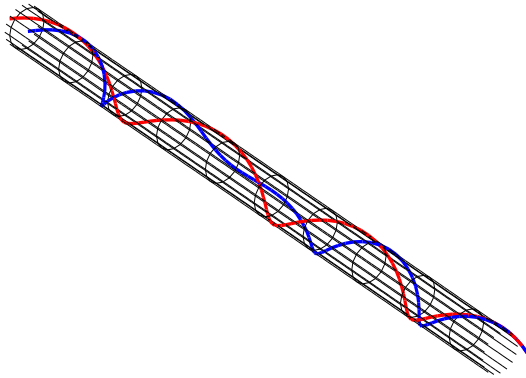


Figure 9. Modes of deformation, **red curve**: $P_{app} = -3.0$ kN after 20 bending cycles, **blue curve**: $P_{app} = -3.25$ kN after 20 bending cycles.

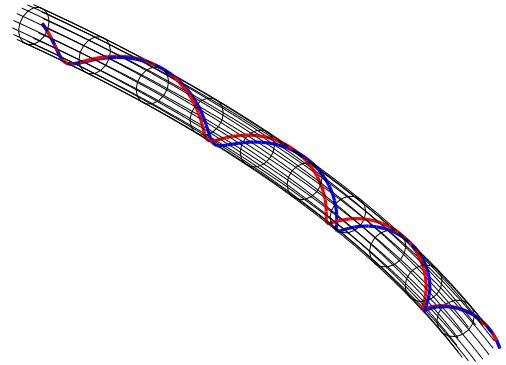


Figure 10. Modes of deformation, **red curve**: $P_{app} = -3.25$ kN, maximum bending, **blue curve**: $P_{app} = -3.25$ kN, maximum bending, first cycles.

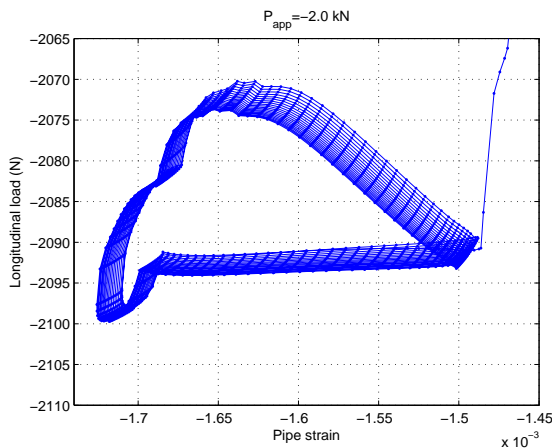


Figure 11. Equilibrium path loop, $P_{app} = -2.0$ kN, $s = S_L/2$.

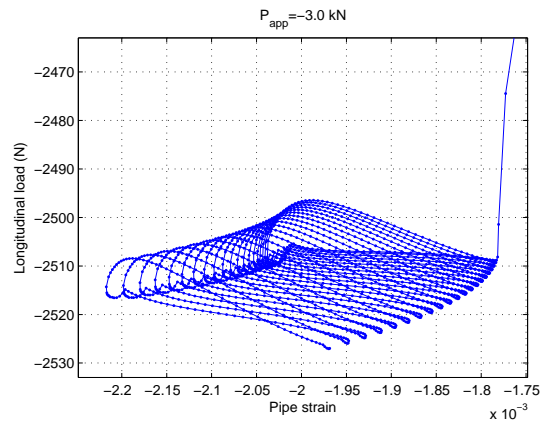


Figure 12. Equilibrium path loop, $P_{app} = -3.0$ kN, $s = S_L/2$.

change of strain after each bending cycle has been concluded with respect to the strain obtained after the first bending cycle will be considered, see Figure 14. The slope of these curves can now be taken as basis for consideration of if the wire will remain in a stable configuration, or if instability may occur after a larger number of bending cycles. The magnitude of slope for the analyses with P_{app} set to -2.0 kN and -2.5 kN is decreasing while this value for the remaining analyses is increasing. The conclusion can therefore be drawn, that the wire for the two first load levels seem to converge against a closed loop in (force-strain)-diagrams, while the geometry of the equilibria obtained with the remaining load levels do not converge towards closed loop behavior. The limit compressive load for the wire can on basis of this method be estimated to lie between 2.5 and 2.75 kN.

It is interesting to compare this measure for the maximum load carrying ability of a single wire with the limit load obtained from a frictionless analysis of both layers of armoring wires by methods proposed in [6]. Calculating the compressive load per wire, an equilibrium path as shown on Figure 15 is obtained. A limit load of -2.33 kN is

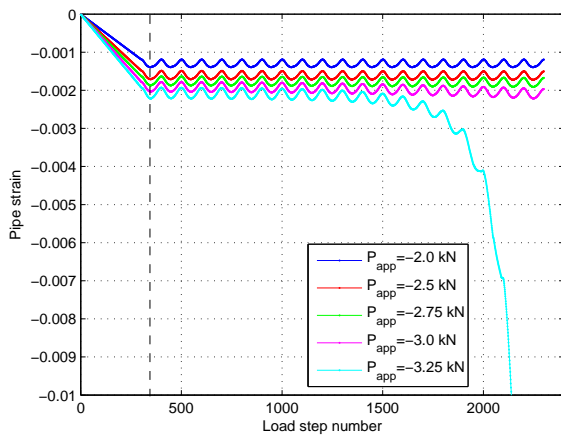


Figure 13. Pipe strains.

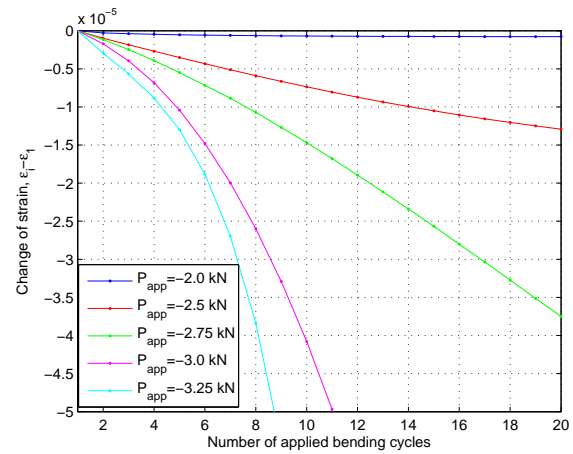


Figure 14. Change of pipe strain.

obtained as maximum load carrying ability by the analysis. This is slightly less than the value determined on basis of the present analysis.

In order to compare the wire mode of deformation associated with instability obtained by the present method with the buckling mode determined with no friction, these are shown in Figure 17. It is noted that the frictionless buckling mode is calculated with a deformation controlled model and that direct comparison of the magnitude of the two responses is not possible. Furthermore, the two responses do not represent the same load level, since this cannot be ensured due to significant differences in the chosen means for controlling the model. However, it can be concluded that the two deformation modes have approximately the same shape. Hence, inclusion of friction in the model can not be concluded to have changed buckling modes significantly. In order to investigate the effect of the frictional coefficient, three analyses with $P_{app} = -2.75$ kN and frictional coefficients 0.05, 0.1 and 0.15 were carried out. The results are available in Figure 16. As expected, the strain rate increases after a lower number of applied bending cycles if the frictional coefficient is decreased.

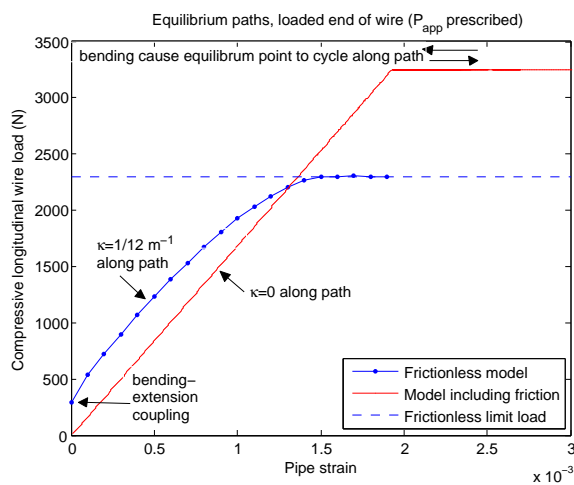


Figure 15. Equilibrium paths of loaded end of wire, analyses with and without friction.

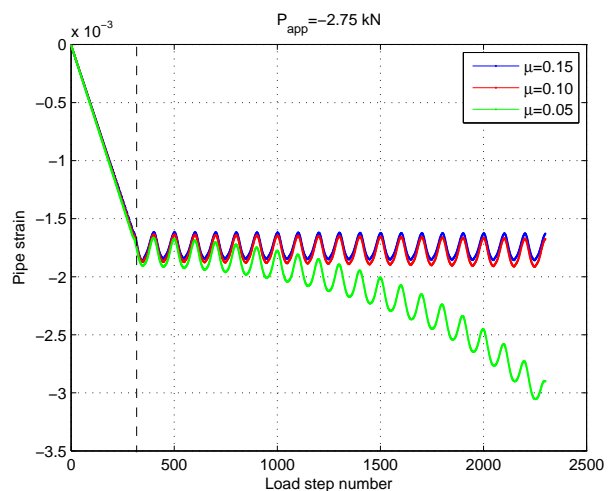


Figure 16. Influence of variation of the frictional coefficient on the pipe strain response.

It is a well-described phenomenon that stick-slip effects in the tensile armour layers cause hysteresic flexural behavior in flexible pipes, see [11] and [13]. In order to investigate, how the present approach to frictional effects on armoring wires corresponds to the descriptions given in other publications, the moment-curvature relation is studied in Figure 18. The total local wire moment \mathbf{M} is calculated on vectorial form as the sum of the moments around the wire tnb -directions. The obtained moment can afterwards be projected onto the z -axis on basis of a unit vector k in this direction.

$$\mathbf{M} = M_t \mathbf{t} + M_n \mathbf{n} + M_b \mathbf{b} \quad M_z = \mathbf{M} \cdot \mathbf{k} \quad (26)$$

The behavior detected by the present approach corresponds well to the expected hysteresic flexural behavior despite only the contribution from a single wire is considered. However, it is noted that a force term should be added in equation 26 if the total contribution from the analyzed wire to the global pipe moment is desired, see [6].

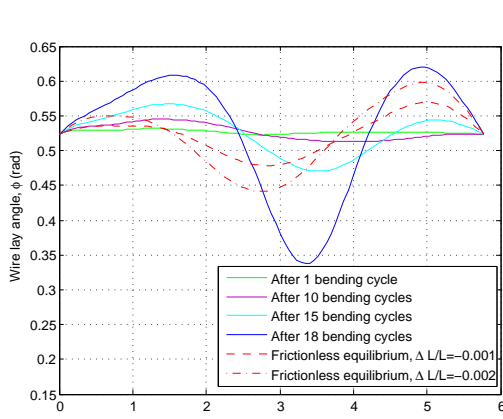


Figure 17. Comparison of deflection modes, wire lay angle, results obtained with and without inclusion of frictional effects.

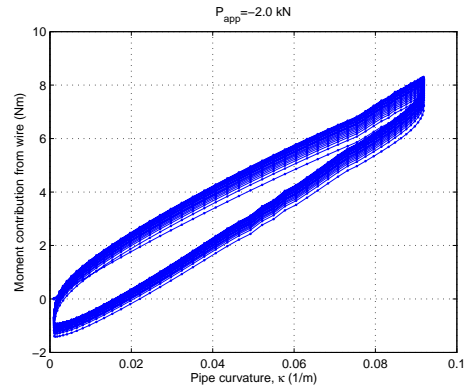


Figure 18. Wire contribution from local moments to global pipe hysteresic flexural behavior for $P_{app} = -2.04$ kN, $s = S_L/2$.

For small wire slips, it is reasonable to calculate slippage in terms of a tangential and a transverse components by projecting the wire slip for load step i onto the initial tangent, \mathbf{t}_0 , and initial binormal, \mathbf{b}_0 for fixed curvature

$$D_t = \|\mathbf{D} \cdot \mathbf{t}_0\| \quad D_b = \|\mathbf{D} \cdot \mathbf{b}_0\|$$

The two slip components are plotted versus each other, see Figure 19 and 20. Similar results are presented in [17] and [21].

Conclusions

On basis of an established model for determination of the equilibrium state of an armoring wire within the wall of a flexible pipe, means for inclusion of frictional effects have been presented. Solutions are obtained as the solution to a boundary value problem solved for each step in a predefined load history. Friction has been modeled as tangential and transverse distributed wire loads with magnitudes based on a regularized Coulomb law and the normal distributed wire load. The directions of the frictional loads have been calculated on basis of the wire slippage with respect to the the previous load step. Despite the choice of slip speed transition is arguable, the proposed method has proven capable

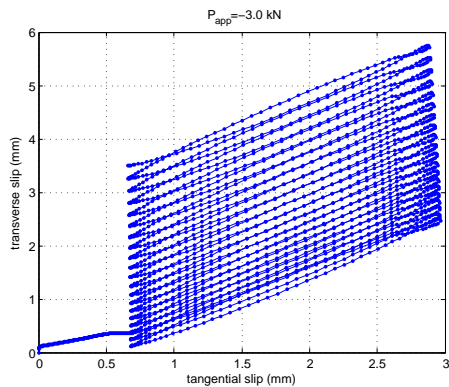


Figure 19. Tangential wire slip vs. transverse wire slip for $P_{app} = -3.0$ kN.

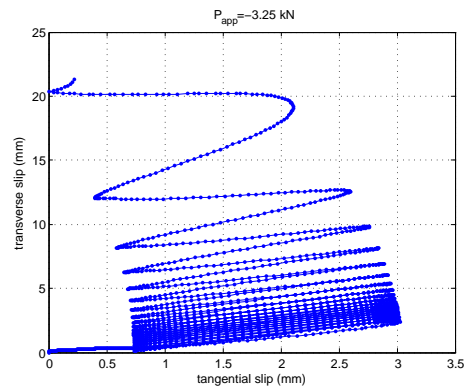


Figure 20. Tangential wire slip vs. transverse wire slip for $P_{app} = -3.25$ kN.

of limiting the wire slippage in dynamic loading and representing key-effects which are known to be caused by friction.

The proposed method was applied to a specified pipe design and the stability of a single wire subjected to prescribed cyclic loads was examined. It was found, that when simulating only a limited number of bending cycles, an estimation of if the wire would remain in a stable configuration could be found by considering the change of strain obtained after each bending cycle with respect to the strain found after the first bending cycle. The slope of the obtained curves may serve as basis for stability considerations, since they reveal if wire slippage converges towards a stable configuration or not. The buckling modes determined were approximately of the same shape as buckling modes found if friction was neglected. The load carrying ability was slightly larger than the limit load determined when friction was neglected.

With larger computational power, than used for conducting the present analyses, the proposed method may be used to model all wires within the wall of a flexible pipe. However, coupling the stick-slip effects to the global flexural pipe constitutive relations, which due to friction is known to exhibit hysteresic behavior leading to variations of the radius of curvature, is a task which calls for further research. Due to the assumption, that the global curvature is constant, this cannot be conducted, without extending the present formulation. Furthermore, it is desirable to investigate means for implementation of a shorter transition zone and possibly a frictional law based on measured parameters. Inclusion of such means in the analysis are likely to limit wire slippage further and represent the modeled physics in a more accurate manner. In order to do so, further research and severe computational power is needed. However, very little research in slip mechanics allowing transverse slips limited by friction has been conducted, and the present research may therefore serve as a valuable basis for further research.

References

- [1] API Spec 17J, Specification for Unbonded Flexible Pipe American Petroleum Institute, 2nd edition, 1999
- [2] Braga, M.P. and Kaleff, P. *Flexible Pipe Sensitivity to Birdcaging and Armor Wire Lateral Buckling*. Proceedings of OMAE, 2004

- [3] Bectarte, F. and Coutarel, A. *Instability of Tensile Armour Layers of Flexible Pipes under External Pressure*. Proceedings of OMAE, 2004
- [4] Secher, P., Bectarte, F. and Felix-Henry, A. *Lateral Buckling of Armor Wires in Flexible Pipes: reaching 3000 m Water Depth*. Proceedings of OMAE, 2011
- [5] Tan, Z., Loper, C., Sheldrake, T. and Karabelas, G. *Behavior of Tensile Wires in Unbonded Flexible Pipe under Compression and Design Optimization for Prevention* Proceedings of OMAE, 2006
- [6] Østergaard, N.H., Lyckegaard, A. and Andreassen, J. *On lateral buckling failure of armour wires in flexible pipes*. Proceedings of OMAE, 2011
- [7] Féret, J.J. and Bournazel, C.L. *Calculation of stresses and slips in structural layers of unbonded flexible pipes*. Journal of Offshore Mechanics and Arctic Engineering, Vol. 109, 1987
- [8] CAFLEX Theory manual. *IFP/SINTEF*, 1991
- [9] McIver, D.B. *A method of modeling the detailed component and overall structural behaviour of flexible pipe sections*. Engineering Structures, Vol. 17, No. 4, pp. 254-266, 1995
- [10] Custódio, A.B. and Vaz, M.A. *A nonlinear formulation for the axisymmetric response of umbilical cables and flexible pipes*. Applied Ocean Research 24, 21-29, 2002
- [11] Alfano, G., Bahtui, A. and Bahai, H. *Numerical derivation of constitutive models for unbonded flexible risers*. International Journal of Mechanical Sciences 51, 295-304, 2009
- [12] Vaz, M.A. and Patel, M.H. *Post-buckling behaviour of slender structures with a bilinear bending moment-curvature relationship*. International Journal of Non-linear Mechanics, Vol. 42, p.470-483, 2007
- [13] Witz, J.A. and Tan, Z. *On the Flexural Structural Behaviour of Flexible Pipes, Umbilicals and Marine Cables*. Marine Structures, Vol. 5, 1992
- [14] Kraincanic I. and Kabadze E. *Slip initiation and progression in helical armouring layers of unbonded flexible pipes and its effect on pipe bending behavior*. Journal of Strain Analysis, Vol. 36, No. 3, 2001
- [15] Out, J. M. M. and von Morgen, B. J. *Slippage of helical reinforcing on a bent cylinder*. Engineering Structures, Vol. 19, No. 6, pp. 507-515, 1997
- [16] Sævik, S. *A finite element model for predicting stresses and slip in flexible pipe armouring tendons*. Computers and Structures. Vol. 46, No.2, 1993
- [17] Leroy, J.M. and Estrier, P. *Calculation of stresses and slips in helical layers of dynamically bent flexible pipes*. Oil and Gas Science and Technology, REV. IFP, Vol. 56, No. 6, pp. 545-554, 2001

- [18] Østergaard, N.H., Lyckegaard, A. and Andreasen, J. *A method for prediction of the equilibrium state of a long and slender wire on a frictionless toroid applied for analysis of flexible pipe structures*. Submitted to Engineering Structures, accepted for publication
- [19] Reissner, E. *On finite deformations of space-curved beams*. Journal of Applied Mathematics and Physics (ZAMP), Vol. 32, 1981
- [20] Love, A.E.H. *A treatise on the Mathematical Theory of Elasticity*. Dover Publications, Inc., N.Y, 1944
- [21] Brack. A., Troina, L.M.B. and Sousa, J.R.M. *Flexible Riser Resistance Against Combined Axial Compression, Bending and Torsion in Ultra-Deep Water Depths*. Proceedings of OMAE, 2005

Niels Højen Østergaard, Anders Lyckegaard
 NKT-Flexibles / Aalborg University, Department of Mechanical and Production Engineering
 Priorparken 480, DK-2605 Broendby
 Niels.HojenOstergaard@nktflexibles.com, Anders.Lyckegaard@nktflexibles.com

Jens H. Andreasen
 Department of Mechanical and Production Engineering, Aalborg University
 Pontoppidanstræde 103, DK-9000 Aalborg
 jha@m-tech.aau.dk

Appendix: Derivation of equations governing the wire equilibrium state

In this section, the methods used for determination of the equilibrium state of an armouring wire within the wall of a flexible pipe are described.

Geometry

A point on the toroid given by a set of (u, θ) -coordinates is in cartesian coordinates given by

$$\mathbf{x}(u, \theta) = \begin{bmatrix} \left(\frac{1}{\kappa} + r \cdot \cos \theta\right) \cos(\kappa u) - \frac{1}{\kappa} \\ \left(\frac{1}{\kappa} + r \cdot \cos \theta\right) \sin(\kappa u) \\ r \cdot \sin \theta \end{bmatrix} \quad (27)$$

A curve α is defined by specifying a relation in (u, θ) -coordinates. Assuming that such a relation is given, the following norms are defined

$$\mathbf{x}_u = \frac{\partial \mathbf{x}}{\partial u} \quad \mathbf{x}_\theta = \frac{\partial \mathbf{x}}{\partial \theta} \quad (28)$$

Assuming the curve parametrized by arclength s , a local curvilinear coordinate triad of orthonormal vectors, tangent \mathbf{t} , normal \mathbf{n} and binormal \mathbf{b} , see Figure 5, can be attached to the curve

$$\mathbf{t} = \frac{d\alpha}{ds} = \mathbf{x}_u \frac{du}{ds} + \mathbf{x}_\theta \frac{d\theta}{ds} \quad \mathbf{n} = \frac{\mathbf{x}_u \times \mathbf{x}_\theta}{\|\mathbf{x}_u \times \mathbf{x}_\theta\|} \quad \mathbf{b} = \mathbf{t} \times \mathbf{n} \quad (29)$$

In equation (29), the wire normal has been defined equal to the surface normal. Hereby, it is assumed that adjacent pipe layers are sufficiently stiff to prohibit the wire from rotating

freely around the local tangent. Hence, the rotation around \mathbf{t} is geometrically governed by the underlying toroid.

Addressing the definition of the wire tangent geometry, an alternative definition can be based on the following vectors spanning the tangent space of the toroid

$$\mathbf{t} = \cos \phi \mathbf{t}_u + \sin \phi \mathbf{t}_\theta \quad (30)$$

in which \mathbf{t}_u and \mathbf{t}_θ , which span the toroid tangent space, are given by

$$\mathbf{t}_u = \frac{\mathbf{x}_u}{\|\mathbf{x}_u\|} \quad \mathbf{t}_\theta = \frac{\mathbf{x}_\theta}{\|\mathbf{x}_\theta\|} \quad (31)$$

In order for this definition to be consistent with equation (29), the following two differential equations must hold

$$\frac{du}{ds} = \frac{\cos \phi}{\|\mathbf{x}_u\|} = \frac{\cos \phi}{1 + r\kappa \cos \theta} \quad \frac{d\theta}{ds} = \frac{\sin \phi}{\|\mathbf{x}_\theta\|} = \frac{\sin \phi}{r} \quad (32)$$

These equations govern the wire geometry in the surface tangent plane.

Transformation formulae

Having defined two orthonormal frames, $(\mathbf{t}, \mathbf{n}, \mathbf{b})$ and $(\mathbf{t}_u, \mathbf{t}_\theta, \mathbf{n})$, see Figure 5, it is desirable to relate those by a transformation formula

$$\begin{bmatrix} \mathbf{t} \\ \mathbf{n} \\ \mathbf{b} \end{bmatrix} = \begin{bmatrix} \cos \phi & \sin \phi & 0 \\ 0 & 0 & 1 \\ \sin \phi & -\cos \phi & 0 \end{bmatrix} \begin{bmatrix} \mathbf{t}_u \\ \mathbf{t}_\theta \\ \mathbf{n} \end{bmatrix} \quad (33)$$

Furthermore, considering the $(\mathbf{t}, \mathbf{n}, \mathbf{b})$ -frame, it is desirable to relate the triad vectors to their derivatives in arclength. Defining a normal curvature component, κ_n (curvature in the (\mathbf{t}, \mathbf{n}) -plane), a geodesic curvature component, κ_g (curvature in the (\mathbf{t}, \mathbf{b}) -plane) and a wire torsion component, τ (in the (\mathbf{n}, \mathbf{b}) -plane), this transformation, known as the Darboux frame, is given by

$$\frac{d}{ds} \begin{bmatrix} \mathbf{t} \\ \mathbf{n} \\ \mathbf{b} \end{bmatrix} = \begin{bmatrix} 0 & \kappa_n & -\kappa_g \\ -\kappa_n & 0 & \tau \\ \kappa_g & -\tau & 0 \end{bmatrix} \begin{bmatrix} \mathbf{t} \\ \mathbf{n} \\ \mathbf{b} \end{bmatrix} \quad (34)$$

It is noted, that the transformation contained in equation (34) implies that a positive rotation about a given triad axis corresponds to a positive change of curvature for a positive change of arclength. This is sufficient to specify the signs in the constitutive relations for the wire.

Equilibrium equations

The equations of equilibrium for a curved Bernoulli-Euler beam segment were formulated by Kirchhoff and included in Love's book on theory of elasticity, [20]. On vectorial form, the equilibrium equations were given by Reissner, [19]

$$\frac{d\mathbf{P}}{ds} + \mathbf{p} = 0 \quad \frac{d\mathbf{M}}{ds} + \mathbf{t} \times \mathbf{P} + \mathbf{m} = 0 \quad (35)$$

in which \mathbf{P} denotes sectional force, \mathbf{M} sectional moments, \mathbf{p} distributed loads and \mathbf{m} distributed moments. These may on components form be written as

$$\begin{aligned}\mathbf{P} &= P_t \mathbf{t} + P_n \mathbf{n} + P_b \mathbf{b} \\ \mathbf{M} &= M_t \mathbf{t} + M_n \mathbf{n} + M_b \mathbf{b} \\ \mathbf{p} &= p_t \mathbf{t} + p_n \mathbf{n} + p_b \mathbf{b} \\ \mathbf{m} &= m_t \mathbf{t} + m_n \mathbf{n} + m_b \mathbf{b}\end{aligned}\quad (36)$$

Equation (35) can now be rewritten on the form

$$\frac{d\mathbf{P}}{ds} + \mathbf{p} = \quad (37)$$

$$P_t \frac{d\mathbf{t}}{ds} + P_n \frac{d\mathbf{n}}{ds} + P_b \frac{d\mathbf{b}}{ds} + \mathbf{t} \frac{dP_t}{ds} + \mathbf{n} \frac{dP_n}{ds} + \mathbf{b} \frac{dP_b}{ds} + p_t \mathbf{t} + p_n \mathbf{n} + p_b \mathbf{b} = 0 \quad (38)$$

$$\frac{d\mathbf{M}}{ds} + \mathbf{m} + \mathbf{t} \times \mathbf{P} = \quad (39)$$

$$M_t \frac{d\mathbf{t}}{ds} + M_n \frac{d\mathbf{n}}{ds} + M_b \frac{d\mathbf{b}}{ds} + \mathbf{t} \frac{dM_t}{ds} + \mathbf{n} \frac{dM_n}{ds} + \mathbf{b} \frac{dM_b}{ds} + m_t \mathbf{t} + m_n \mathbf{n} + m_b \mathbf{b} - P_b \mathbf{n} + P_n \mathbf{b} = 0 \quad (40)$$

in which the crossproduct $\mathbf{t} \times \mathbf{P}$ is given by

$$\mathbf{t} \times \mathbf{P} = \mathbf{t} \times (P_t \mathbf{t} + P_n \mathbf{n} + P_b \mathbf{b}) = P_t \mathbf{t} \times \mathbf{t} + P_n \mathbf{t} \times \mathbf{n} + P_b \mathbf{t} \times \mathbf{b} = P_n \mathbf{b} - P_b \mathbf{n}$$

The equations of equilibrium can now be written on the following form

$$\frac{dP_t}{ds} + P_n \mathbf{t} \cdot \frac{d\mathbf{n}}{ds} + P_b \mathbf{t} \cdot \frac{d\mathbf{b}}{ds} + p_t = 0 \quad (41)$$

$$\frac{dP_n}{ds} + P_t \mathbf{n} \cdot \frac{d\mathbf{t}}{ds} + P_b \mathbf{n} \cdot \frac{d\mathbf{b}}{ds} + p_n = 0 \quad (42)$$

$$\frac{dP_b}{ds} + P_t \mathbf{b} \cdot \frac{d\mathbf{t}}{ds} + P_n \mathbf{b} \cdot \frac{d\mathbf{n}}{ds} + p_b = 0 \quad (43)$$

$$\frac{dM_t}{ds} + M_n \mathbf{t} \cdot \frac{d\mathbf{n}}{ds} + M_b \mathbf{t} \cdot \frac{d\mathbf{b}}{ds} + m_t = 0 \quad (44)$$

$$\frac{dM_n}{ds} + M_t \mathbf{n} \cdot \frac{d\mathbf{t}}{ds} + M_b \mathbf{n} \cdot \frac{d\mathbf{b}}{ds} - P_b + m_n = 0 \quad (45)$$

$$\frac{dM_b}{ds} + M_t \mathbf{b} \cdot \frac{d\mathbf{t}}{ds} + M_n \mathbf{b} \cdot \frac{d\mathbf{n}}{ds} + P_n + m_b = 0 \quad (46)$$

Applying the transformation given in equation 34, the following expressions are derived

$$\begin{aligned}\kappa_n &= \mathbf{n} \cdot \frac{d\mathbf{t}}{ds} = -\mathbf{t} \cdot \frac{d\mathbf{n}}{ds} \\ \kappa_g &= \mathbf{t} \cdot \frac{d\mathbf{b}}{ds} = -\mathbf{b} \cdot \frac{d\mathbf{t}}{ds} \\ \tau &= \mathbf{b} \cdot \frac{d\mathbf{n}}{ds} = -\mathbf{n} \cdot \frac{d\mathbf{b}}{ds}\end{aligned}\quad (47)$$

The wire curvature components can now be calculated on basis of the chosen geometry

$$\kappa_n = -\frac{\kappa \cos \theta}{1 + r\kappa \cos \theta} \cos^2 \phi - \frac{1}{r} \sin^2 \phi \quad (48)$$

$$\kappa_g = \left(\frac{\kappa \sin \theta}{1 + r\kappa \cos \theta} \cos \phi + \frac{d\phi}{ds} \right) \quad (49)$$

$$\tau = \left(\frac{\kappa \cos \theta}{1 + r\kappa \cos \theta} - \frac{1}{r} \right) \cos \phi \sin \phi \quad (50)$$

Constitutive relations

In order to relate the changes of curvature with respect to the initial helical wire state ($\kappa = 0$) to sectional wire moments, the constitutive relations will be assumed linear. This is a reasonable assumption if the wire cross sectional dimensions are small compared to the minor torus radius, which is the case when modeling a flexible pipe. Furthermore, it will be assumed that the wire strains, ϵ , are small, so Cauchy's definition of strain applies. The following constitutive relations can then be assumed valid

$$\begin{aligned} P_t &= EA\epsilon & M_t &= GJ\Delta\tau \\ M_b &= EI_b\Delta\kappa_n & M_n &= EI_n\Delta\kappa_g \end{aligned}$$

Similar constitutive relations have to a wide extend been applied when investigating the mechanics of armouring wires, see [8, 13, 17].

Field equations

In order to determine the geometry of the wire which on basis of the chosen constitutive relations satisfy the equations of equilibrium, a sixth order system of first order differential equations can be derived by considering the following:

- Equation (32) governing the wire geometry in the toroid tangent plane provides two differential equations in u and θ .
- The definition of the geodesic curvature, equation (49), provides one differential equation in ϕ .
- The equilibrium equations in tangential force, equation (41), in binormal force, equation (43) and normal moment, equation (45), provides three differential equations in P_t , P_b and M_n .

This yields the system of six first order differential equations (1-6).